Far-infrared Graphene Plasmonic Crystals for Plasmonic Band Engineering

— SUPPORTING INFORMATION —

Kitty Y. M. Yeung[1,†], Jingyee Chee[1,†], Hosang Yoon[1], Yi Song[2],
Jing Kong[2] and Donhee Ham[1,*]

[1]School of Engineering and Applied Sciences, Harvard University, Cambridge, MA 02138, USA.
[2]Department of EECS, Massachusetts Institute of Technology, Cambridge, MA 02139, USA.
[†] These authors contributed equally.
[*] Corresponding author. Email: donhee@seas.harvard.edu

S1 Symmetry-Based Plasmonic Band Selection Rule

Our graphene plasmonic crystals are realized by creating hexagonal lattices of apertures in continuous graphene media. The hexagonal lattice—whether its aperture is circularly or hexagonally shaped—possesses the C_{6v} point group symmetry with 6-fold rotation axes and 6 reflection planes; see Fig. S1 in case of the hexagonal lattice with circular apertures. Following the crystallographic convention, we denote the 12 symmetry operations (elements) constituting the group as E, C_6 ($\times 2$), C_3 ($\times 2$), C_2, σ_y ($\times 3$), and σ_x ($\times 3$). The 6 irreducible representations of the C_{6v} group are denoted as A_1, A_2, B_1, B_2, E_1, E_2, also following the convention. The character table of the C_{6v} group is in Table S1.

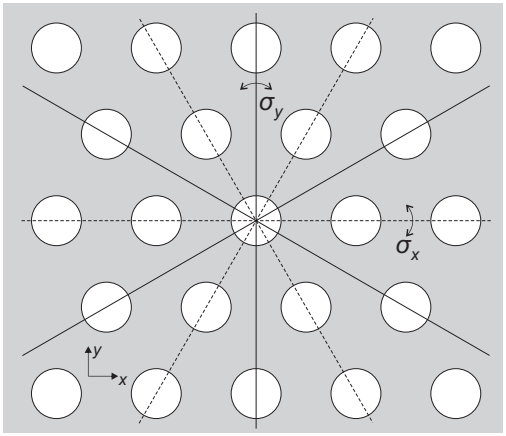

Figure S1: Point group symmetry of the hexagonal lattice.

The structural symmetry of the hexagonal lattice leads to the physical symmetry of the plasmonic waves hosted by the structure[1]. The plasmonic dynamics in the lattice is governed by the electromagnetic wave equation. Its stationary solutions represent plasmonic eigenmodes, which, for $k_p = 0$, become the Γ-point plasmonic modes on different plasmonic bands, as discussed in the main text. The fields of these Γ-point plasmonic eigenmodes manifest definite spatial symmetry properties under any operation belonging to the C_{6v} group; this is evident from, for example, the $E_{p,z}$

C_{6v}	E	$2C_6$	$2C_3$	C_2	$3\sigma_y$	$3\sigma_x$
A_1	1	1	1	1	1	1
A_2	1	1	1	1	-1	-1
B_1	1	-1	1	-1	1	-1
B_2	1	-1	1	-1	-1	-1
E_1	2	1	-1	-2	0	0
E_2	2	-1	-1	2	0	0

Table S1: Character table of the C_{6v} point symmetry group.

spatial profiles of the Γ-point modes right above GPC1, shown in Fig. 2c of the main text. Formally, the symmetric transformation properties of any given non-degenerate Γ-point plasmonic eigenmode or any given set of degenerate Γ-point plasmonic eigenmodes are described uniquely by one of the 6 irreducible representations of the C_{6v} group. For GPC1, for example, the 11 lowest-lying Γ-point modes can be classified as in Table S2, based on the irreducible representations that describe their symmetry transformation properties.

Band indices of Γ-point plasmonic eigenmodes	2	3	4	5,6 (degenerate)	7	8	9	10, 11 (degenerate)
Irreducible representation	E_2	E_2	B_1	E_1	B_2	E_2	E_2	E_1

Table S2: Classification of the Γ-point plasmonic eigenmodes of GPC1.

This assignment of a plasmonic eigenmode to a unique irreducible representation in Table S2 is done as follows. Consider, as an example, the non-degenerate Γ-point plasmonic mode on band 4 for GPC1 (f = 5.7 THz; Figs. 2a and 2c, main text). By inspection of the spatial profile of $E_{\mathrm{p},z}$ of this mode (Fig. 2c, main text), we see that a 60° rotation of $E_{\mathrm{p},z}$ about the z-axis flips its sign, *i.e.*,

$$C_6(E_{\mathrm{p},z}) = -E_{\mathrm{p},z}, \tag{1}$$

and a reflection of $E_{\mathrm{p},z}$ along the y-axis maintains the field component, *i.e.*,

$$\sigma_y(E_{\mathrm{p},z}) = E_{\mathrm{p},z}. \tag{2}$$

These relations identify the characters of C_6 and σ_y operations on the band-4 Γ-point mode as -1 and 1, respectively. By juxtaposing these results with Table S1, we see that the symmetry properties of this Γ-point mode are uniquely described by irreducible representation B_1.

As another example, for doubly-degenerate Γ-point modes on bands 5 & 6 for GPC1 (f = 6.8 THz; Figs. 2a and 2c, main text), each operation of the C_{6v} group may be expressed as a 2×2 matrix. For instance, a 180° rotation of the $E_{\mathrm{p},z}$ fields of the degenerate modes about the z-axis flip their signs (Fig. 2c, main text), which can be expressed as

$$C_2 \begin{pmatrix} E_{5,\mathrm{p},z} \\ E_{6,\mathrm{p},z} \end{pmatrix} = \begin{pmatrix} -1 & 0 \\ 0 & -1 \end{pmatrix} \begin{pmatrix} E_{5,\mathrm{p},z} \\ E_{6,\mathrm{p},z} \end{pmatrix}. \tag{3}$$

Thus the character of C_2—the trace of the 2×2 matrix on the right hand side—for these doubly-degenerate modes is -2. By resorting to Table S1, we then see that the symmetry properties of these degenerate Γ-point modes on bands 5 and 6 can be described only by irreducible representation $E1$. In this way, we complete Table S2.

Next, we consider the physical symmetry of the excitation plane waves that are normally incident. The symmetry properties of these free-space light waves can be also identified uniquely with one of the irreducible representations of the C_{6v} group in exactly the same manner as above. Firstly, they are doubly degenerate due to the two orthogonal

polarizations, and secondly, 180° rotations about the z-axis flip the signs of their fields, *i.e.*:

$$C_2 \begin{pmatrix} E_{\text{light},\,x} \\ E_{\text{light},\,y} \end{pmatrix} = \begin{pmatrix} -1 & 0 \\ 0 & -1 \end{pmatrix} \begin{pmatrix} E_{\text{light},\,x} \\ E_{\text{light},\,y} \end{pmatrix}. \tag{4}$$

Therefore, the character of C_2 for the doubly-degenerate free-space waves is -2, just like the doubly-degenerate Γ-point plasmonic modes on bands 5 & 6, and thus, the symmetry properties of the free-space radiation are described uniquely by the E_1 irreducible representation.

Finally, as we look at Table S2, we see that among all the 11 lowest-lying Γ-point plasmonic modes of GPC1, the symmetry properties of only those on bands 5 & 6 and 10 & 11, are described by the E_1 irreducible representation, just like the symmetry properties of the normally-incident excitation plane waves. In other words, only these particular plasmonic modes respond in the same way as the normally-incident plane waves under the symmetry operations of the C_{6v} group. This is the reason why only these specific Γ-point plasmonic modes are coupled to (and excited by) the free-space radiation, even though all Γ-point modes satisfy the phase matching condition.

S2 Simulated Extinction Spectra of All Four Graphene Plasmonic Crystals

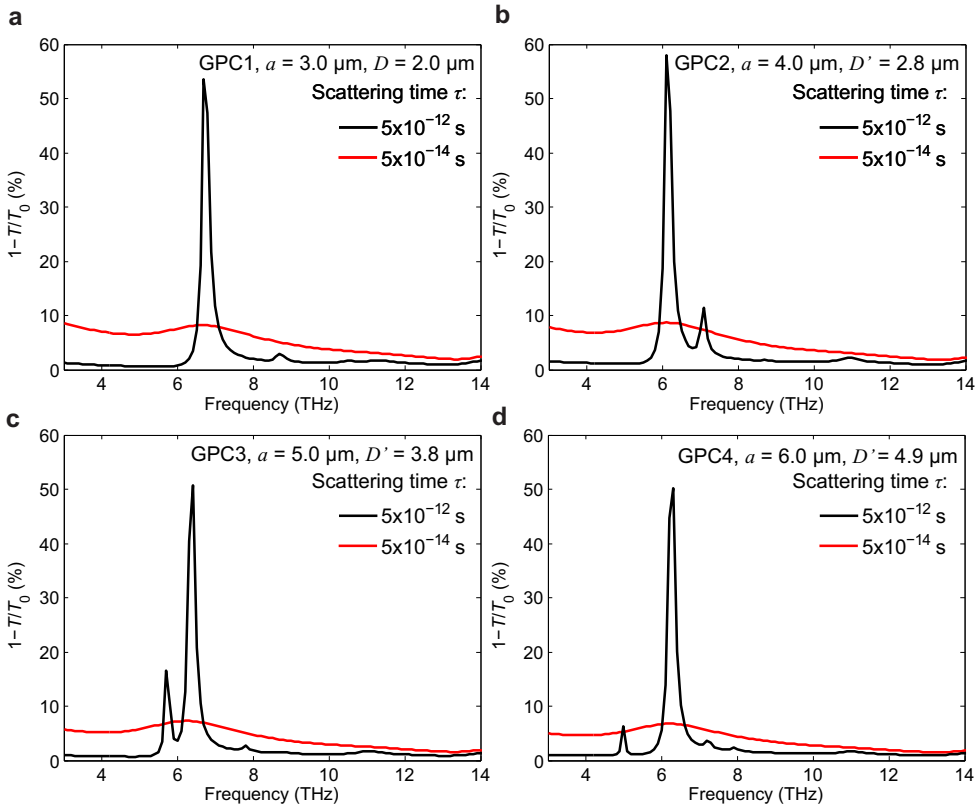

Figure S2: Simulated extinction spectra of GPC1-GPC4. $E_{\text{F}} = -0.38$ eV is used.

The main text discussed the simulated extinction spectra of GPC1 only. Figure S2 presents the simulated extinction spectra for all 4 plasmonic crystals we implement in the experiment. The same behavior is observed all across the 4 crystals. Firstly, when the carrier scattering time τ is large (5×10^{-12} s), multiple plasmonic peaks emerge in the

extinction spectra, where these peaks correspond to the subsets of Γ-point plasmonic modes, chosen by the symmetry-based selection rule (Sec. S1). Secondly, as τ is reduced to 5×10^{-14} s, which is commensurate with the mobility of our CVD-grown graphene, in each crystal, the previously smaller peaks become blurred and the previously dominant peak remains resolvable (sometimes with a small frequency shift), while it becomes shorter and broader. In summary, in all plasmonic crystals, with the carrier scattering time realistic with the CVD-grown graphene, a single broad peak emerges, as firmly demonstrated experimentally in the main text.

S3 Calculated Extinction Spectra of Unpatterned Graphene

The extinction spectrum of the unpatterned graphene sheet on the SiO_2/Si substrate in the N_2 atmosphere is calculated using the scattering matrix method through a N_2/graphene/SiO_2/Si/N_2 stack. Scattering matrices are constructed by calculating the transmission and reflection coefficients at the material interfaces and propagation factors accounting for phase delay and attenuation through different material layers[2]. The material properties needed in these calculations are obtained from tabulated data[3]; the free charge carrier conductivity σ of graphene also needed for these calculations is found in the main text. The monotonic extinction spectrum calculated in this way compares well to the measured extinction spectrum of unpatterned graphene (Fig. S3), which confirms that the monotonic spectrum is due to the background interaction between the light and free charge carriers in graphene.

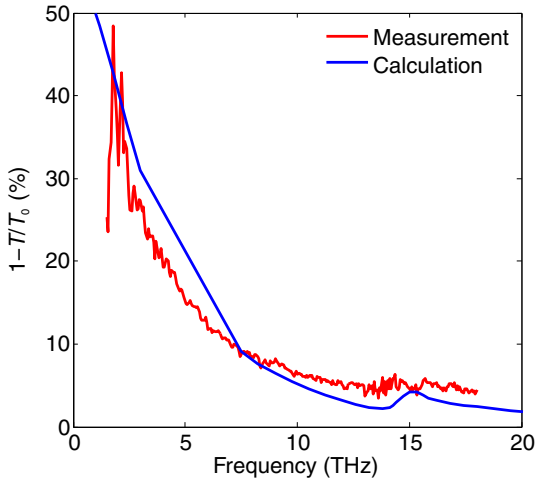

Figure S3: Measured (red) and calculated (blue) extinction spectra of an unpatterned graphene sheet. $E_F = -0.38$ eV and $\tau = 5 \times 10^{-14}$ s measured in the unpatterned region are used in the calculation.

S4 Spectral Dependency on the Hexagonal Lattice Geometry

In the experiments presented in the main text, our device setup did not allow us to examine the dependence of the extinction spectra *purely* on the lattice geometry, partly because the photolithography cannot perfectly control the shape and size of the apertures as designed, and mainly because E_F varies from crystal to crystal. Thus in this section, we examine the pure geometry dependency of the extinction spectrum theoretically, resorting to simulations.

To begin with, we consider GPC1-type plasmonic crystals—hexagonal lattice with circular apertures—as demonstrational vehicles (Fig. S4). Simulations show that for an increasing a with a fixed D/a—this represents a simple

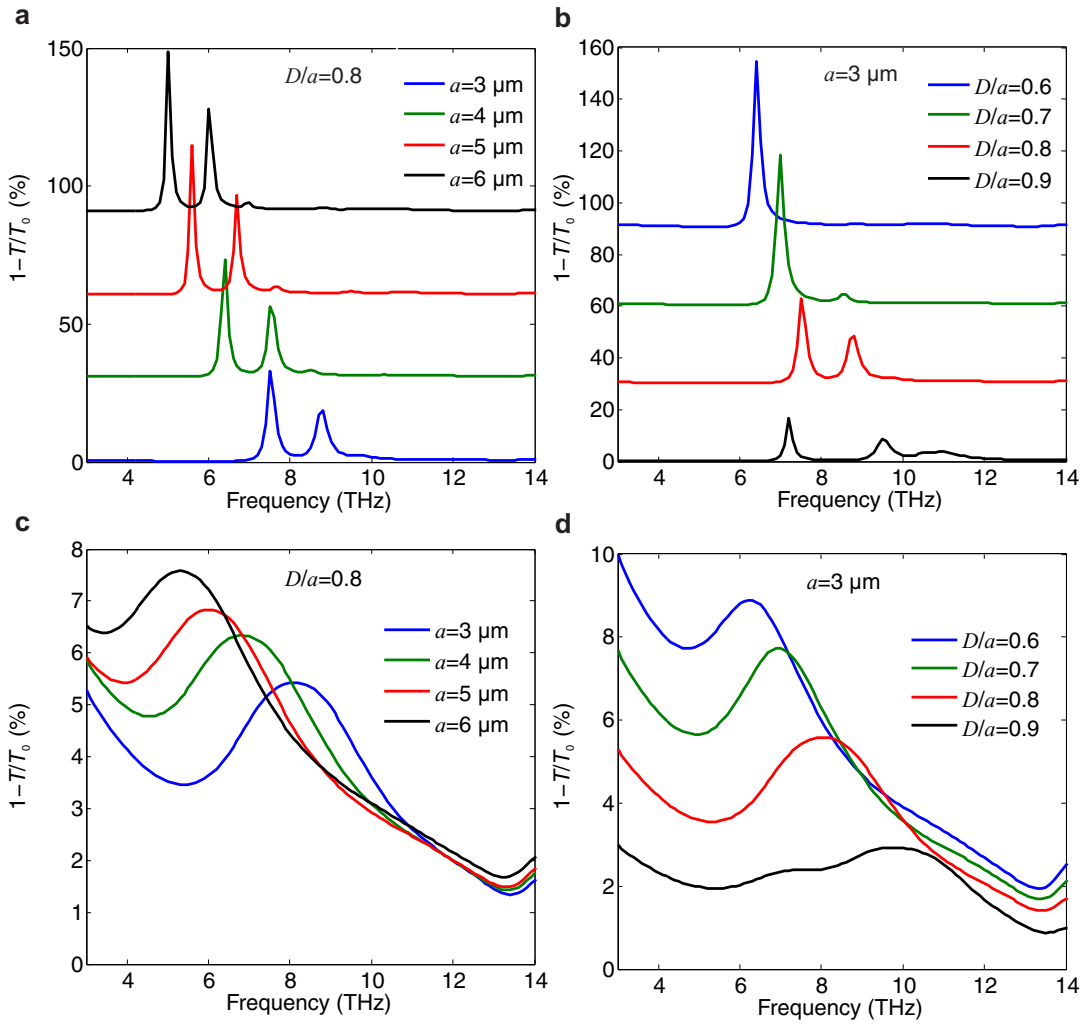

Figure S4: Simulated extinction spectra of circular-aperture hexagonal lattices with varying D and a. $\tau = 5 \times 10^{-12}$ s for **a, b**; $\tau = 5 \times 10^{-14}$ s (as in CVD graphene) for **c, d**. $E_F = -0.38$ eV is used for all simulations.

scaling of the crystal, *i.e.*, the hexagonal lattice and its inner structural details are stretched by the same factor in all directions—, both the multiple plasmonic peak frequencies in the weak scattering regime (Fig. S4a) and the single plasmon peak frequency in the heavy scattering regime decrease (Figs. S4c). This is explained as follows. As the plasmonic wavenumbers k_p's at Brillouin zone boundaries are inversely proportional to the lattice constant a, the Brillouin zones become smaller with the increasing a, while the approximate relation $f \propto \sqrt{k_p}$ is maintained *within* Brillouin zones, regardless of the increasing a. Therefore, for a larger value of a, the plasmonic bands cross both the Brillouin zone boundaries and the Γ points at lower frequencies. Therefore, the extinction peaks appear at lower frequencies with the increasing a.

When D is increased for a fixed a (we choose $a = 3$ μm here)—this corresponds to the change in the inner structure of the lattice, although the aperture shape remains to be circular—, the extinction spectrum changes in a more complicated manner. In the low scattering regime ($\tau = 5 \times 10^{-12}$ s; Fig. S4b), for $D/a = 0.6$, a single peak appears, but as D/a is increased, second and even third peaks emerge in the extinction spectra, and the frequency of the original single peak first increases and then decreases back. These richer behaviors reflect that as the inner structure of the lat-

tice is changed, the band structure—and thus the subset of Γ-point plasmonic modes that satisfy the symmetry-based selection rule—is altered in a complex manner, as expected. In the heavy scattering regime ($\tau = 5 \times 10^{-14}$ s; Fig. S4d), while the second and third peaks are largely blurred out, the behavior of the original single peak (that is now broadened) remains the same with the increasing D for a fixed a; its frequency first increases, and then decreases back.

From the study of the foregoing paragraph, we can expect that the change of the aperture shape—another way of modifying the inner structure of the lattice—will also alter the band structure (and thus the extinction spectra) in a complex manner. To demonstrate, we compare a hexagonal lattice with circular apertures ($a = 6$ μm, $D = 5$ μm) and a hexagonal lattice with hexagonal apertures ($a = 6$ μm, $D' = 5$ μm; GPC4). In the weak scattering regime (Fig. S5a), the positions and resonance strengths of multiple plasmonic peaks differ in nontrivial ways between the extinction spectra of the two lattices. It follows that in the heavy scattering regime (Fig. S5b), the single plasmonic peaks occur at two noticeably differing frequencies.

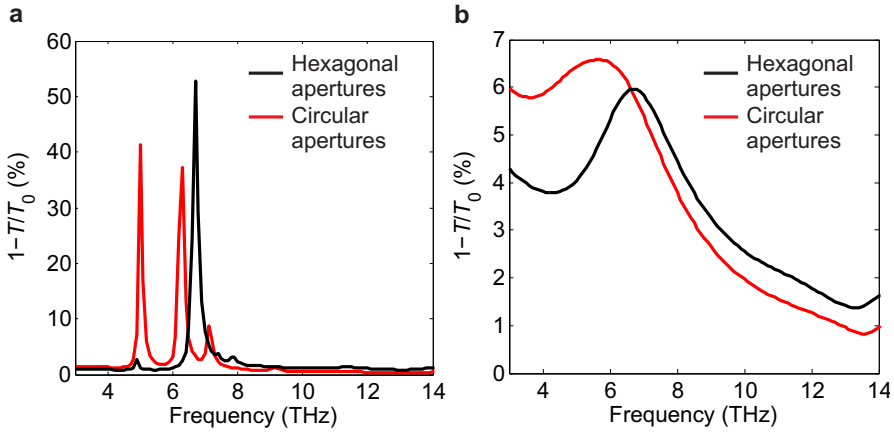

Figure S5: Simulated extinctions for a hexagonal lattice with circular apertures ($a = 6$ μm, $D = 5$ μm) and a hexagonal lattice with hexagonal apertures ($a = 6$ μm, $D' = 5$ μm). $\tau = 5 \times 10^{-12}$ s for **a**; $\tau = 5 \times 10^{-14}$ s for **b**; $E_F = -0.38$ eV.

These studies show that the plasmonic band structure can be richly manipulated by means of the crystal geometry. This is a powerful feature for plasmonic band engineering, and will become even more useful, as the control of the spatial variation of the Fermi level of large-area graphene further improves.

References

(1) Sakoda, K. *Optical Properties of Photonic Crystals, 2nd Edition*; Springer: Berlin, 2005.

(2) Crassee, I.; Orlita, M.; Potemski, M.; Walter, A. L.; Ostler, M.; Seyller, T.; Gaponenko, I.; Chen, J.; Kuzmenko, A. B. *Nano Lett.* **2012**, *12*, 2470–2474.

(3) Palik, E. D. *Handbook of Optical Constants of Solids*; Academic Press Inc: New York, 1985.